



OPEN Spinal cord neuromodulation for blood pressure control using low-intensity focused ultrasound

Angelica F. Lopez^{1,2}, Denis Routkevitch^{1,2,3}, Patrick J. Kramer^{2,3}, Neil A. Babu¹, Ritvik Jillala^{2,3}, Ananya Tandri¹, Zoe Soulé¹, Emily C. Baca¹, A. Daniel Davidar^{2,3}, Vikas N. Vattipally^{2,3}, Pierce L. Perkins¹, Siddharth Krishnan^{2,3}, Ryan S. Bohluli¹, Charles G. Eberhart⁴, Betty M. Tyler³, Nicholas Theodore^{1,2,3,5,6}, Nitish V. Thakor^{1,2,7} & Amir Manbachi^{1,2,3,7,8,9}✉

Focused ultrasound (FUS) is an innovative technology that delivers angled acoustic energy to a small target region. Previous FUS technology has demonstrated efficacy in applications such as tumor destruction, nerve modulation, and drug delivery in the brain. We investigated the effects of low-intensity FUS (LIFU) stimulation on the spinal cord and its ability to regulate mean arterial pressure (MAP). We found that LIFU stimulation on exposed rat spinal cord could modulate MAP, causing a decrease when applied at a lower thoracic level and an increase when applied at a lumbosacral level. We also found that shorter stimulation periods (30 s) were more effective in inducing a decrease in MAP than more extended stimulation periods (90 s). The time required to return to baseline for MAP was shown to increase with subsequent periods of FUS stimulation. FUS could enable non-pharmacological, spatially targeted MAP control, especially for impaired patients. Future applications of FUS neuromodulation extend into solutions for clinical blood pressure disorders, such as autonomic dysreflexia or chronic hypertension.

Keywords Blood pressure, Focused ultrasound, Mean arterial pressure, Neuromodulation, Spinal cord, Stimulation

Abbreviations

AD	Autonomic dysreflexia
BP	Blood pressure
FUS	Focused ultrasound
HIFU	High-intensity focused ultrasound
LIFU	Low-intensity focused ultrasound
MAP	Mean arterial pressure
SCI	Spinal cord injury

In the United States alone, 48.1% of adults have high blood pressure (BP)¹. Worldwide cases of hypertension are near 1.28 billion adults². As a result, BP management has become an essential aspect of modern healthcare^{3–7}. Current methods of managing hypertensive BP primarily rely on pharmacological agents; however, these pharmacological agents can have many adverse effects, including hypotension, cephalgia, and vertigo^{8,9}. In an effort to develop clinical alternatives to pharmacological BP management, we investigated focused ultrasound (FUS) stimulation as a novel approach to manipulate mean arterial pressure (MAP). MAP is the average of the BP waveform over time^{10,11}. MAP is commonly utilized to estimate systemic blood flow. It is a metric for

¹Department of Biomedical Engineering, Johns Hopkins University, Baltimore, MD, USA. ²HEPIUS Innovation Lab, Johns Hopkins University, Baltimore, MD, USA. ³Department of Neurosurgery, Johns Hopkins University, Baltimore, MD, USA. ⁴Department of Clinical and Laboratory Pathology, Johns Hopkins University, Baltimore, MD, USA. ⁵Department of Orthopedic Surgery, Johns Hopkins University, Baltimore, MD, USA. ⁶Department of Pediatrics, Johns Hopkins University, Baltimore, MD, USA. ⁷Department of Electrical and Computer Engineering, Johns Hopkins University, Baltimore, MD, USA. ⁸Department of Anesthesiology and Critical Care, Johns Hopkins University, Baltimore, MD, USA. ⁹Department of Mechanical Engineering, Johns Hopkins University, Baltimore, MD, USA. ✉email: amir.manbachi@jhu.edu

the management of chronic health conditions and in the evaluation of tissue perfusion in potentially ischemic conditions such as traumatic brain injury and spinal cord injury^{10,12,13}.

Focused ultrasound is an effective and inexpensive method for targeted delivery of energy. It focuses ultrasonic energy onto a single site to cause tissue effects^{14–16}. High-intensity FUS (HIFU) has demonstrated clinical safety and efficacy in applications including tumor ablation and targeted drug delivery^{17–22}. Low-intensity FUS (LIFU) has been successfully implemented for neuromodulation^{23–26}, peripheral nerve stimulation^{27–29}, and transient crossing of the blood–brain barrier^{30–33}. Although FUS has been implemented on other physiological sites, its application for MAP management has been minimal³⁴.

This study aims to demonstrate the modulation of MAP with FUS stimulation of the spinal cord. Our previous studies provided us with preliminary data and limitations in FUS stimulations of the spinal cord, namely the inability to have live visualization of the FUS^{35,36}. We use a custom-designed transducer mounted in a 3D-printed frame that can be integrated with conventional ultrasound. This allowed us to achieve live visualization of FUS with concurrent real-time blood flow imaging. In the study, we characterized changes in MAP from FUS stimulation in two regions along the exposed rat spinal cord: at a lower thoracic region and at a lumbosacral region. Finally, we evaluated histological staining samples to characterize tissue effects and confirm the effectiveness of FUS stimulation.

Our group had two hypotheses. The first hypothesis was that stimulation with FUS on the spinal cord would elicit a change in blood pressure. The second hypothesis was that different regions along the spinal cord would elicit different changes in MAP based on the degree of innervation from sympathetic and parasympathetic pathways. We varied the positioning of the coaxial imaging setup along the spinal cord to better understand the varied mechanisms of neuromodulation.

Materials and methods

Imaging setup

It was critical to have consistency between the alignment of the focal point of the H-107 FUS probe with a central aperture (Sonic Concepts Inc.) and the conventional i22LH8 probe (Canon Inc., center frequency 20 MHz)³⁷. The H-107 FUS probe is a 0.5 MHz focused transducer, with a 64.0 mm active diameter with a 63.2 mm radius of curvature, fundamental focal length of 21.42 mm, and fundamental focal width of 3.02 mm. This FUS transducer had a central rectangular opening (Fig. 1A). This is because we wanted accurate live visualization of the FUS focal point in the anatomical landscape. Key acoustic indices for the focused transducer are outlined in Table 1 and Supplemental Table 1. The coaxial imaging setup consisted of a 3D-printed FUS cone and a 3D-printed upper clamp (Elegoo Saturn 3) to house the coaxial imaging probe, with the i22LH8 imaging probe positioned within the rectangular aperture (Fig. 2).

To power the coaxial imaging setup, we connected a series of electrical components. A 33500B Series Trueform Waveform Generator (Keysight Technologies) was programmed for each frequency and amplitude parameter in MATLAB. A 240L RF Amplifier (Electronics & Innovation Inc.) was connected to the output of the Waveform Generator, which was then connected to the input of the paired fundamental resonance impedance matching network for the FUS probe. A matching network (consisting of step-up transformers) was designed to match a driver electronics input impedance of 50 Ω to SonicConcept's H-107 focused ultrasound transducer (center frequency: 500 kHz).

Pressure intensity simulations

A k-Wave acoustic simulation³⁸ of the transducer's theoretical beam profile was conducted to estimate and evaluate the acoustic energy at the spinal cord depth delivered by the FUS transducer. Simulation transducer parameters were designed to match experimental transducer values and are specified in Table 2. The acoustic beam profile was measured across an 80 mm cubic medium with generic soft tissue acoustic parameters ($c = 1540$ m/s, $\rho = 1000$ kg/m³) to capture the target stimulation depth of interest. An ellipse rod-shaped spinal cord was modeled at the transducer target focal depth of 51.54 mm to literature-determined dimensions^{39,40} and acoustic parameters⁴¹, specified in Table 3. A continuous wave transmittance with ramp-up of 4 periods was simulated across a 100 μ s total time interval. The maximal pressure outputs of the simulation were measured to compare the pressure characteristics upon inclusion of the spinal cord.

Animals

All animal experiments were conducted in compliance with the National Institutes of Health guide for the care and use of laboratory animals (NIH Publications No. 8023, revised 1978). The experimental protocols were approved by the Johns Hopkins University Animal Care and Use Committee. All methods were performed following the ARRIVE guidelines (Animal Research: Reporting of In Vivo Experiments). Eight female Sprague Dawley rats (11 weeks, Charles River Laboratories) and 1 male Yorkshire pig (70–75 kg, Oak Hill Genetics) were used for this study. Each rat was allocated to either thoracic or lumbosacral laminectomy. The choice of sex and age were based on literature model standards in the field⁴². This study utilized female Sprague Dawley rats as our group has an established model with these rats and found it efficient to perform the postoperative care and bladder expression⁴³.

Intubation and ventilation

Rats were intubated for constant and stable anesthesia. The rats were placed on an intubation stage and intubated with standard technique. A rat intubation kit was used (Kent Scientific). Several lidocaine drops were administered to the rat's vocal cords to avoid laryngospasm, and a 14 G angiocatheter was advanced into the trachea. The rat was then connected to the RoVent respirator (Kent Scientific) and placed on the surgical stage and maintained on isoflurane anesthesia. Isoflurane concentration was maintained at 2.2–2.5% during intubation

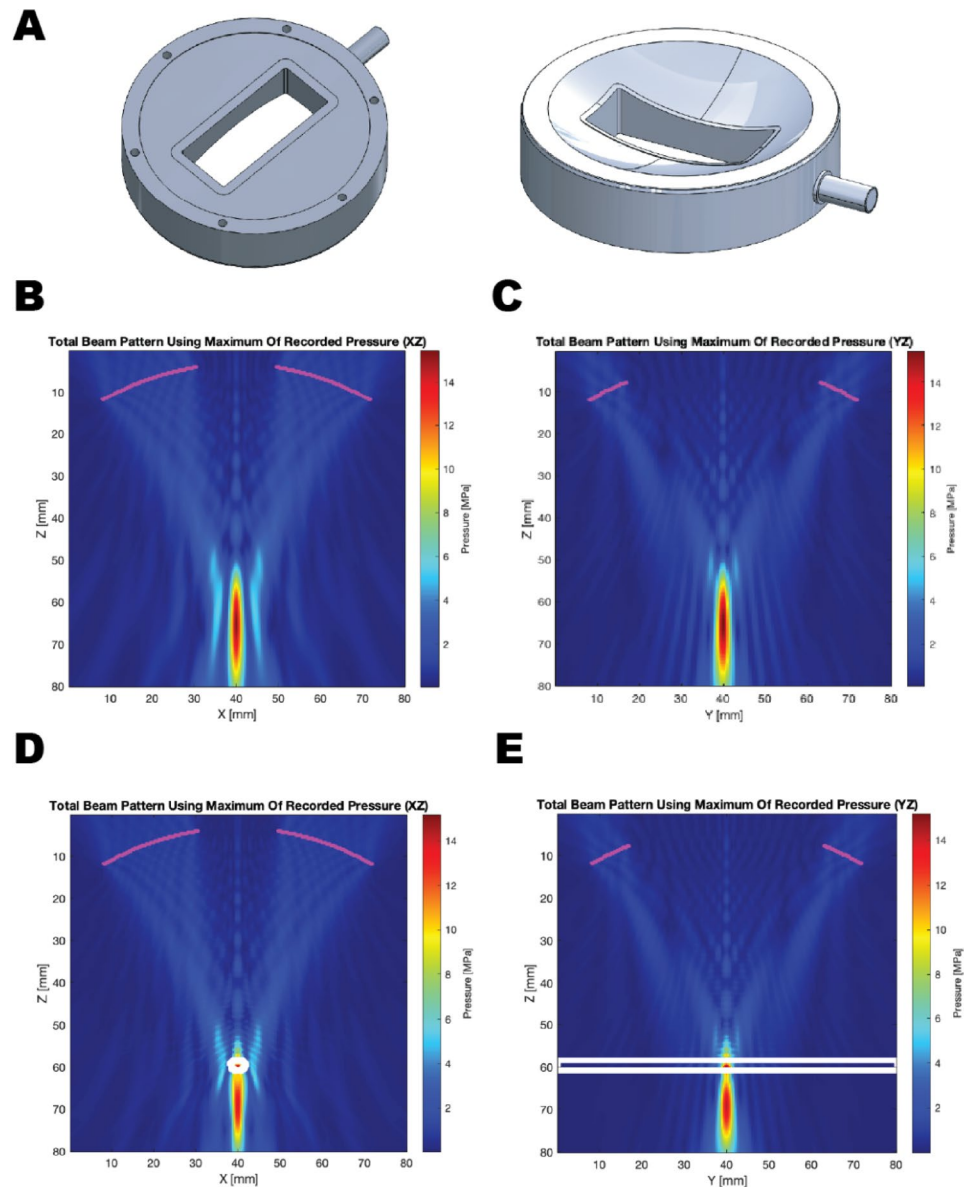


Fig. 1. k-Wave simulation renderings of the transducer. **(A)** Two CAD orientations show the top (left) and bottom (right) of the custom coaxial FUS transducer. **(B, C)** The ‘true’ beam profile of the FUS transducer in a soft tissue medium with no inclusions. The max pressures for the XZ and YZ planes are included. **(D, E)** The maximal beam profile is illustrated for FUS in the spinal medium, with the spinal cord at the focal depth of the transducer. The spinal cord outline is overlaid in white and the FUS transducer outline is overlaid in magenta.

Hydrophone transducer acoustic indices	
Central frequency	500 kHz
Spatial peak pulse average intensity (I_{sppa})	1.19 W/cm ²
Peak negative pressure (PNP)	−0.18 MPa
Mechanical index (MI)	0.26
Thermal index (TI)	0.95

Table 1. Physical transducer acoustic indices. Specifies the focused transducer model parameters obtained from hydrophone scan.

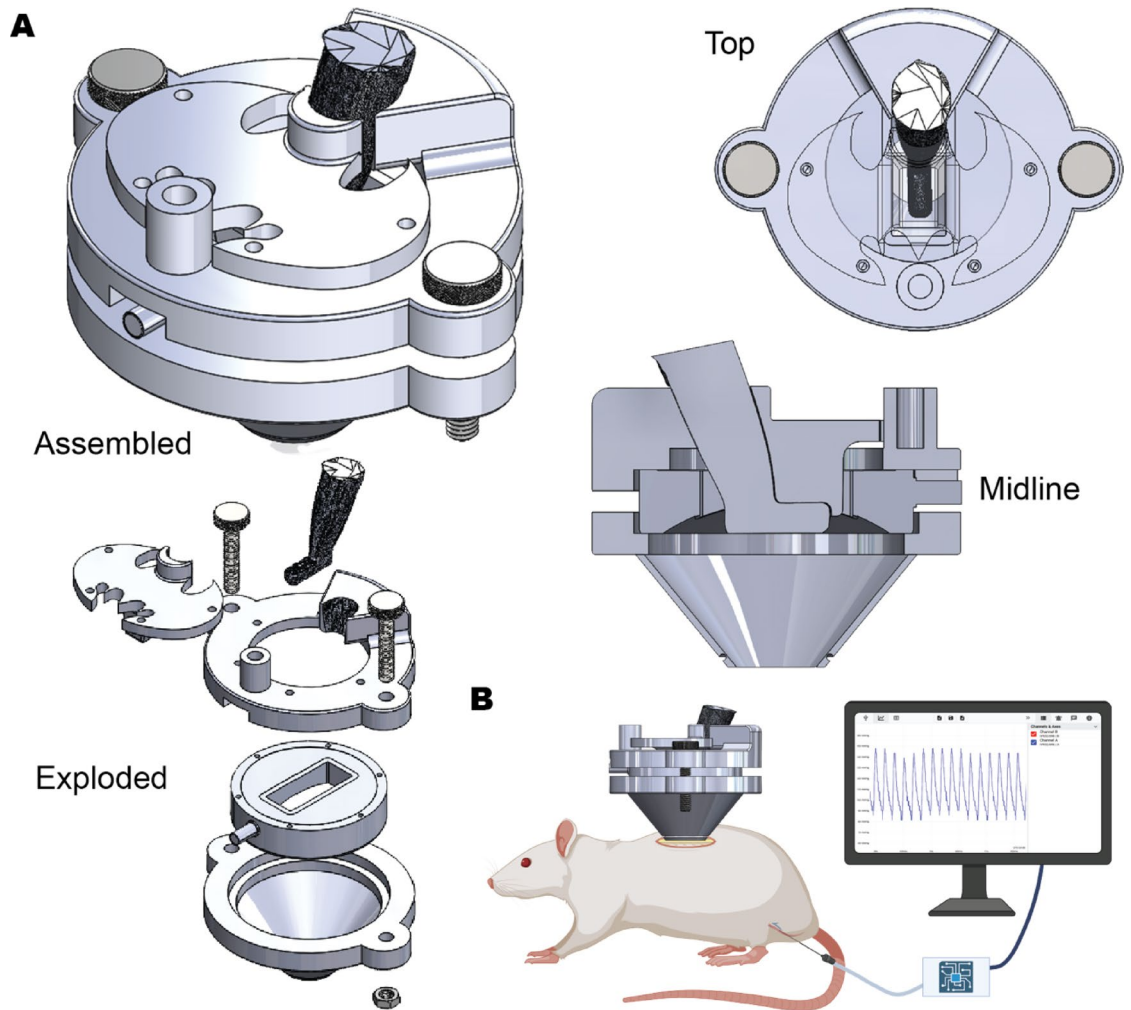


Fig. 2. Coaxial FUS transducer and commercial ultrasound imaging probe enable precise targeting of the spinal cord in real-time. **(A)** Computer-aided design renderings of the coaxial FUS and ultrasound imaging setup illustrated in an assembled format, top-down view of FUS transducer and commercial ultrasound probe alignment, exploded format, and midline view for part visualization for FUS in the spinal cord. **(B)** Illustration of the coaxial FUS and ultrasound imaging setup over exposed spinal cord with a representative BP recording. Created in BioRender. Thakor, (2025) <https://BioRender.com/itb5fd5>.

k-Wave transducer model	
Array diameter	64 mm
Central frequency	500 kHz
Central opening (rectangular)	45.49 mm × 18.59 mm
Maximum surface pressure	1.102 MPa

Table 2. Simulated transducer properties. Specifies the focused transducer model parameters used in the k-Wave modeling.

and then lowered to 1.5–1.8% during surgical procedures. Anesthesia concentration, tidal volume, respiratory rate, and end-expiratory pressure were managed at standard values calculated based on weight. Respiratory rate was maintained at approximately 60 breaths per minute.

The pig was intubated following normal veterinary protocol. Following this, the pig was placed on a ketamine (30 mg/kg) and xylazine (3 mg/kg) mixture for initial anesthesia. Subsequent use of inhaled isoflurane (0.5–2.5%) on a ventilator and continuous infusion of fentanyl (0.03–0.2 mg/kg/hr) was done for the duration of the surgical procedure. Throughout the experiment, anesthesia concentration, tidal volume of 5–10 mL/kg, respiratory rate of 17–22 breaths per minute were managed. Pig temperature was maintained at 37.2–38.3 °C. Intravenous saline was administered at 3 mL/kg/hr.

k-Wave tissue model	Soft tissue	Spinal cord
Speed of sound	1540 m/s	1542 m/s
Density	1000 kg/m ³	1075 kg/m ³
Attenuation coefficient	0.75 Db/MHz/cm	0.8 Db/MHz/cm
Dimensions	–	3.5 mm × 2.5 mm ellipse

Table 3. Simulated tissue parameters. Specifies the acoustic absorption/attenuation coefficient of the spinal cord and attenuation of surrounding medium used in the k-Wave modeling.

Arterial catheterization

All rats underwent an arterial catheterization of the femoral artery for MAP recordings. Briefly, the skin above the femoral artery was incised and blunt dissection was used to expose the femoral artery and vein. A 4–0 silk suture was fed around the artery and used to occlude the artery distally. A temporary clamp was then placed on the proximal end of the artery, providing a small, 5 mm region of the artery for the catheter positioning and placement. Before the catheter incision was made, drops of lidocaine were administered onto the artery to prevent vasospasm. The 30 G catheter was filled with heparinized saline and then advanced approximately 2 cm through the small incision. Once the catheter was properly positioned, the temporary clamp was removed and the catheter was secured with suture.

The pig underwent arterial catheterization which was done according to standard protocol. Briefly, the skin above the femoral artery was incised and the catheter was introduced to the artery with a 5 Fr introducer set (Micropuncture Introducer Set, Cook Medical). Arterial blood pressure was measured using a 6 Fr femoral arterial catheter (Fast-Cath, Abbott Cardiovascular). Once placed, this catheter was sutured to the skin and connected to the central monitoring system.

Laminectomy

All rats underwent laminectomy to expose the spinal cord. Rat anesthesia was regulated with the intubation described above. Isoflurane concentration was monitored and adjusted to the physiological metrics of the rat, including respiratory rate and paw pinch reflex. The T13 vertebra was localized with palpation of the ribs, identifying the last floating ribs of the rat. For rats undergoing a lower thoracic laminectomy, the T11–T13 vertebral levels were exposed. This vertebral level was initially chosen for the large size of the vertebrae and based on previous work in spinal cord injury (SCI) rat models⁴⁴. Alternatively, rats undergoing a lumbosacral laminectomy had the L5–S1 vertebrae localized and exposed. This vertebral level was chosen for the large size of the vertebrae and based on previous literature⁴⁵.

Similarly, the pig underwent 2 laminectomies to expose the thoracic spinal cord; an upper and lower thoracic laminectomy were performed to help evaluate the effectiveness of selected FUS stimulation parameters for decreasing MAP.

FUS targeting

Initial calibration of the transducer was done with a Y-120 hydrophone (Sonic Concepts) placed in a pressure tank (Supplemental Fig. 1). These scans determined the depth of the focal point along with a profile for the pressure intensity fields in both the X and Y axial planes. For each rat, the FUS transducer was prepared for targeting. The 3D-printed coaxial FUS imaging system was mounted with a stereotactic frame above the exposed spinal cord. The B-mode display guided the positioning of the focal point. The FUS focal point can be seen from the intraoperative monitor (Supplemental Fig. 2).

FUS intensity parameters

The parameters involved in the coaxial modulation included (i) voltage amplitude (mVpp), (ii) stimulation frequency (kHz), (iii) stimulation period (sec), (iv) duty cycle %, and (v) pulse duration (msec). The center frequency of the probe is 500 kHz and has a range of 321 to 708 kHz (77% bandwidth: (708–321)/500). A complete list of rat parameter combinations used and the number of instances can be found in Supplemental Tables 2, 3 and 4. Multiple stimulation parameters were employed in each rat, with “wash-out” time provided between stimulations to minimize summation effects. The order of stimulation parameters, such as stimulation intensity and durations, were randomized within each rat.

With the 2 laminectomies in the pig, we were able to deliver a range of FUS parameters, varying the intensity and duty cycle of the stimulation between HIFU (500 mVpp, 50–100%) and LIFU (100–250 mVpp, 1–30%). Given the pig’s larger anatomy, we were more capable of visualizing the effects of the FUS stimulation on the spinal cord and surrounding tissue, ultimately aiding in our translation to the clinic. A complete list of pig parameter combinations used and the number of instances can be found in Supplemental Table 5.

Euthanasia

All animals were euthanized in accordance with the experimental protocols approved by the Johns Hopkins University Animal Care and Use Committee. The rats were euthanized through the inhaled carbon dioxide method as standard per the institutional guidelines and confirmed through cervical dislocation.

The pig was euthanized with a 390 mg/ml intravenous injection of Euthasol (pentobarbital sodium and phenytoin sodium).

Spinal cord histology

Following euthanasia, all spinal cords were collected and fixed in formalin prior to histology embedding, sectioning, and staining. Samples were kept refrigerated for storage and future processing. Spinal cord samples were processed by the Johns Hopkins Oncology Tissue Services. Collected spinal cord samples were fixed for 24 to 48 h using 4% paraformaldehyde at 4 °C. After fixation, spinal cord samples were processed and embedded in paraffin. These were then sectioned at 5 μm thickness and stained in accordance with standard hematoxylin and eosin (H&E) histological methods. Samples were assessed for hemorrhage and neuronal damage.

Signal processing

MATLAB R2024a (MathWorks) and Python were used for all analyses and plots. All MATLAB scripts will be available on GitHub. Raw BP data was first processed in MATLAB script and filtered for vertical resolution enhancement. Systolic pressure (SP), diastolic pressure (DP), and MAP were calculated and used in finding averages. FUS stimulation periods were overlaid with MAP plots (Fig. 3). Maximum change during FUS stimulation and mean change during FUS stimulation per parameter was also extrapolated from the BP data using MATLAB. Delta FUS was calculated using a MATLAB script that extracted MAP values at the start and end of the stimulation period. The difference between these values was divided by the stimulation duration to determine delta FUS. Data were categorized based on unique combinations of amplitude, stimulation period, and duty cycle across all experimental subjects, with any excluded data points filtered out before analysis. Exclusion was determined via a filtering MATLAB script to identify time points where the arterial line was flushed. The script computed delta FUS for each unique group and generated graphical representations to visualize the results.

The return to baseline timing was determined using a MATLAB script. To establish the baseline, the script extracted MAP values from 2 s preceding the first of 6 stimulations, which shared the same amplitude, stimulation period, and duty cycle. After all stimulations were completed, the time at which the MAP signal returned to within 5% of the baseline was identified. The return time was calculated by subtracting this time value from the end of the final stimulation. If the MAP signal did not return to baseline before the onset of a subsequent set of stimulations, the return time was adjusted to coincide with the start of the following stimulation sequence.

For the exponential fitting of the signal, the MATLAB script identified the intervals for each FUS stimulation. The script then determined the scaling coefficient (a) and decay rate (b) for each interval. Each fitting underwent an optimization step before saving the curve. Once all intervals had been individually fitted, an average fit was generated for each individual rat and for the overall fit across all experiments. The average fittings were calculated for both lower thoracic and lumbosacral stimulation.

BP signals were analyzed to assess the relationship between BP fluctuations and heart rate variability (HRV). Raw BP waveforms were preprocessed using a fourth-order Butterworth bandpass filter (1–200 Hz for rats; 1–150 Hz for pigs) to reduce baseline drift and high-frequency noise. A 50 Hz notch filter was applied to suppress power-line interference. Systolic peaks were then identified to enable reliable pulse detection, and peak-to-peak intervals were calculated as the time differences between successive systolic peaks. Instantaneous heart rate was derived from peak-to-peak intervals.

After completion of these steps, MAP tracings were manually inspected to classify the effect of FUS into one of four groups: 1. Increase, defined as a minimum 10 mmHg rise in MAP from baseline sustained throughout the stimulation period; 2. Increase with Decompensation, defined as an initial increase followed by subsequent decline of at least 5 mmHg below the peak value, 3. Decrease, defined as a minimum 10 mmHg decrease in MAP

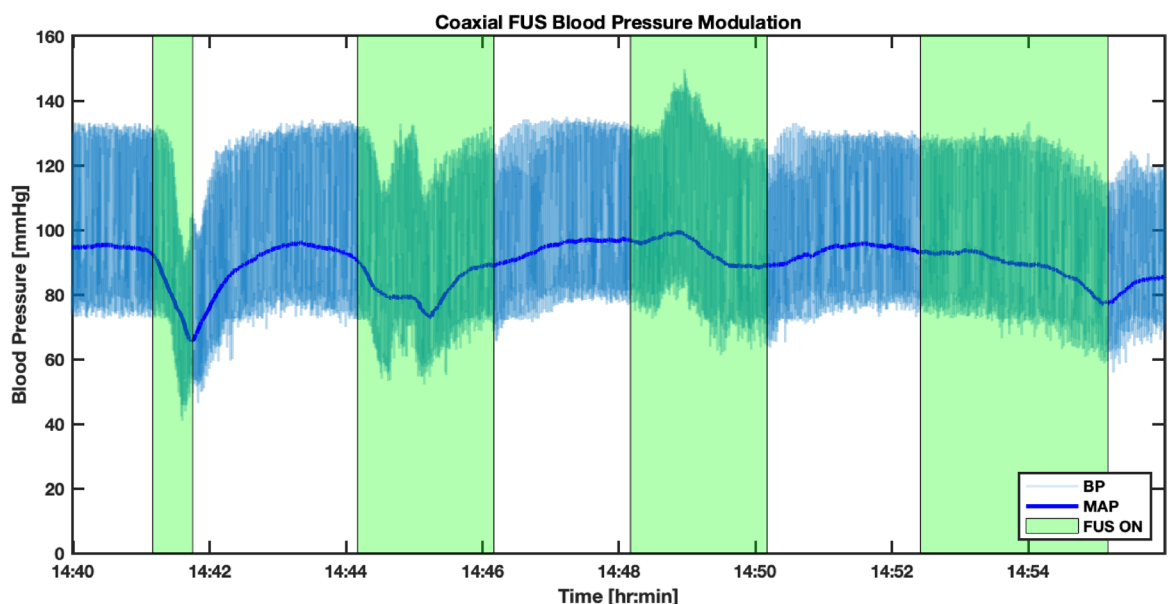


Fig. 3. Representative plot of BP modulation with FUS in thoracic spinal cord. Green bars overlay on a BP and MAP plot to indicate the time and duration of FUS stimulation.

from baseline sustained throughout the stimulation period; and 4. Decrease with Compensation, defined as an initial decrease followed by a rebound of at least 5 mmHg towards the baseline.

Statistical analysis

GraphPad Prism version 10.2.3 (GraphPad) and R (version 4.2.2) were used for all statistical analysis. Statistical significance was assessed using a one-way between-subjects ANOVA with $\alpha=0.05$, assuming a Gaussian distribution. Due to small sample sizes per experimental condition, a between-subjects one-way ANOVA was employed rather than the originally planned repeated-measures design. A post-hoc t-test with Tukey correction was performed to identify significant differences between conditions, applying an adjusted alpha level of 0.05. Finally, we performed a Chi-squared test to assess statistical significance in the frequencies of various event classifications between the stimulated regions. Due to small counts in some observations, the Fisher exact test was used to confirm significance.

Results

Beam profile characterization

Comprehensive characterization of the FUS transducer beam profile was essential for its implementation in biological tissue, such as the spinal cord. The coaxial transducer was modeled in MATLAB using k-Wave and illustrated the pressure intensity of the transducer. Figure 1 demonstrates the total beam pattern and the pressure intensity of the transducer with a 500 kHz center frequency and a 250 mVpp amplitude. The simulation results illustrated the transformation of the beam profile from unobstructed propagation in saline solution (Fig. 1B, C) to the acoustic field distortion observed when overlaid on spinal cord tissue (Fig. 1D, E). The modeled beam profiles illustrate a maximal focal gain of approximately 15 with reference to the surface acoustic pressure of the transducer. The addition of the spinal cord did not substantially change the expected beam profile, with a demonstrated difference in acoustic pressure of less than 1 Pa localized below the spinal structure.

A hydrophone scan of the focused transducer provided intensity and pressure plots of the focal region (Supplemental Fig. 3). Through this scan, key acoustic parameters were obtained and calculated. Specifically, the focused transducer delivered a spatial peak pulse average intensity (I_{sppa}) and mechanical index (MI) of 1.19 W/cm² and 0.26 respectively (Table 1). These LIFU values and those in Table 1 follow the ITRUSST consortium checklist (Supplemental Table 1)^{46,47} and are within the recommended thresholds of focused ultrasound safety per the FDA ($I_{\text{sppa}} = 190$ W/cm² and MI=1.9)^{48,49}. The spatial peak temporal average intensity (I_{spta}) for each stimulation parameter are reported alongside the stimulation tables (Tables 4 and 5; Supplemental Tables 2, 3, 5, 6, and 7). LIFU stimulations were classified as those with duty cycles below 50%. Only FUS stimulations at 100% duty cycle yielded I_{spta} values greater than the recommended LIFU guidelines, thereby falling into a HIFU category. Duty cycles exceeding 50% were used to test whether the observed phenomenon could be replicated under higher intensity conditions.

Quantification of MAP change in a rat model

Here, we present the implementation and outcomes of FUS stimulation on a naïve exposed spinal cord. Using the previously described coaxial setup on the above-mentioned rat model (Fig. 2), we FUS stimulated at 2 spinal vertebral levels: the lower thoracic spinal cord and the lumbosacral spinal cord. Initial observations showed that the stimulations modulated MAP (Fig. 3). Lower thoracic stimulation steadily lowered MAP (Fig. 4A), whereas lumbosacral stimulation caused a noticeable increase (Fig. 4B).

The initial site of stimulation was at the lower thoracic vertebral level (T11-T13). We stimulated 4 rats, which yielded 82 instances of stimulation. Stimulation was done with repeated alternation between a FUS stimulation period and a washout period over several hours per rat. The washout periods allowed sufficient time for rats to return to baseline and for stimulation effects to dissipate. At the lower thoracic spinal cord, the FUS stimulation yielded a Decrease in MAP for 61% of 82 instances (Fig. 4A). There was a subsequent 26% of lower thoracic events that had Decrease With Compensation. Meaning, an overall 87% of FUS stimulation events yielded a type of decrease in MAP. The mean change in MAP following FUS stimulation was further quantified at the lower thoracic spinal cord level. Using one-way between-subjects ANOVA, the data was evaluated for the 4 stimulation durations: 15, 30, 60, and 90 s. Analysis showed that a 30-s FUS stimulation period was more effective at inducing a neuromodulatory change in MAP than a 90-s FUS stimulation period ($P=0.0005$; Fig. 5).

Based on the findings of FUS stimulations at the lower thoracic level, positioning along the spinal cord was further evaluated to understand the ability of FUS to modulate MAP. Four additional rats were stimulated, which yielded 61 instances of stimulation. At the lumbosacral vertebral level (L5-S1), the FUS stimulation showed an Increase in MAP for 38% of 61 instances (Fig. 4B). There was an additional 16% of lumbosacral events that had an Increase With Decompensation. In total, 54% of FUS stimulations at the lumbosacral spinal cord reflected a type of increase in MAP.

To quantitatively measure the physiological phenomenon observed, the following parameters were assessed: (i) the average change during the first 15 s of each group (Supplemental Table 4), (ii) the maximum mmHg change during FUS (Tables 4 and 5), (iii) the average total mmHg changed following FUS (Tables 4 and 5), and (iv) the mean time window for rebound following FUS stimulation (Supplemental Tables 6 and 7). Furthermore, frequencies of each event type are presented in Fig. 6. Statistical significance was observed across spinal region using both the Chi-squared test ($P<0.001$) and Fisher's exact test ($P<0.001$).

Evaluation of neuromodulatory effect in rat

The FUS stimulation parameters, including center frequency, amplitude, stimulation period, duty cycle, and pulse duration, were varied across the course of these studies. To characterize the effect of the FUS stimulation, we narrowed the period of evaluation to the first 15 s of FUS stimulus to assess the increase or decrease of

Amplitude (mVpp)	Stimulation period (sec)	Duty cycle (%)	Pulse duration (msec)	Mean change in MAP (mmHg/sec)	I_{spta} (W/cm ²)	Mean change in MAP during FUS (mmHg)	Maximum decrease in MAP during FUS (mmHg)
100	90	1	1	0.01	0.01	-4.08	-22.37
100	90	5	1	0.00	0.06	-1.02	-12.22
150	15	100	0	-0.13	1.19	3.34	-12.51
150	30	100	0	-0.14	1.19	-3.30	-25.29
150	60	100	0	-0.10	1.19	-9.21	-26.53
200	15	100	0	-0.53	1.19	1.58	-10.98
200	30	50	1	-0.19	0.60	-24.94	-34.32
200	30	100	0	-0.44	1.19	-16.77	-52.24
200	60	50	1	-0.09	0.60	-4.44	-4.45
200	60	100	0	-0.37	1.19	-32.85	-46.40
250	15	50	2000	-0.12	0.60	9.17	5.98
250	15	100	0	-0.42	1.19	-15.42	-37.66
250	30	5	1	-0.01	0.06	-8.20	-20.98
250	30	10	1	-0.18	0.119	-14.87	-38.35
250	30	15	1	-0.03	0.18	3.82	-9.17
250	30	20	1	-0.70	0.24	-16.12	-34.32
250	30	25	1	-0.69	0.30	-33.28	-63.77
250	30	50	1	-1.20	0.60	-37.17	-50.99
250	30	50	2000	-0.11	0.60	-4.79	-8.34
250	30	100	0	-0.63	1.19	-16.36	-39.88
250	60	5	1	-0.02	0.06	-26.61	-35.43
250	60	10	1	-0.28	0.12	-25.56	-25.56
250	60	15	1	-0.23	0.18	-35.15	-39.60
250	60	20	1	-0.37	0.24	-35.64	-35.71
250	60	25	1	-0.57	0.30	-49.05	-52.38
250	60	50	1	-0.48	0.60	-38.69	-59.46
250	60	50	2000	-0.00	0.60	-4.03	-12.50
250	60	100	0	-0.32	1.19	-19.15	-44.19
250	90	1	1	-0.01	0.01	13.55	4.86
250	90	5	1	-0.08	0.06	-16.31	-40.99
250	90	15	1	-0.23	0.18	-20.01	-25.29
250	90	20	1	-0.21	0.24	-20.01	-38.07
250	90	25	1	-0.08	0.30	5.07	3.62
250	90	100	0	-0.08	1.19	-13.69	-24.60
500	90	1	1	-0.06	0.01	14.31	7.50
500	90	5	1	-0.30	0.06	-35.29	-35.29

Table 4. Average lower thoracic spinal cord responses to focused ultrasound stimulation. Displays the following parameters for each set of conditions: (i) average change in MAP (mmHg) per each second that FUS is on, (ii) I_{spta} value, (iii) average change in MAP for total stimulation period, and (iv) the maximum decrease in MAP from FUS stimulation. FUS stimulation period can span 15 to 90 s.

MAP. Individual FUS stimulations lasted 15, 30, 60, or 90 s. From these varied periods, we found the largest change in MAP over time (mmHg/s). At the lower thoracic level, we found that an I_{spta} of 0.24 W/cm², center frequency of 500 kHz, amplitude of 250 mVpp, stimulation period of 30 s, duty cycle of 20%, and pulse duration of 1 ms yielded the greatest change in MAP per second of stimulation (Table 4). This group also correlated with an average decrease of 10.49 mmHg for the first 15 s of FUS stimulation, the largest for the thoracic spinal cord (n = 4 rats) (Supplemental Table 4). At the lumbosacral level, we found that an I_{spta} of 0.30 W/cm², center frequency of 500 kHz, amplitude of 250 mVpp, stimulation period of 30 s, duty cycle of 25%, and pulse duration of 1 ms yielded the most notable change in MAP per second of stimulation (Table 5). This group correlated with an average increase of 2.14 mmHg for the first 15 s of FUS stimulation, the largest for the lumbosacral spinal cord (n = 4 rats) (Supplemental Table 4). Notably, these I_{spta} values are within the recommend FDA guidelines (max I_{spta} = 0.72 W/cm²)⁴⁹. The thoracic parameters evaluated in this study yielded a maximum decrease of 64 mmHg (Table 4) while the lumbosacral parameters yielded a maximum increase of 58 mmHg (Table 5).

Amplitude (mVpp)	Stimulation period (sec)	Duty cycle (%)	Pulse duration (msec)	Mean change in MAP (mmHg/sec)	I_{spta} (W/cm ²)	Mean change in MAP during FUS (mmHg)	Maximum increase in MAP during FUS (mmHg)
250	30	1	1	0.03	0.01	-9.75	5.14
250	30	5	1	-0.00	0.06	7.52	57.94
250	30	10	1	0.03	0.12	7.11	38.76
250	30	15	1	-0.01	0.18	-6.89	18.89
250	30	20	1	-0.02	0.24	-5.42	5.28
250	30	25	1	0.14	0.30	-18.76	-18.76
250	60	1	1	-0.09	0.01	6.81	43.77
250	60	5	1	-0.01	0.06	-8.09	24.59
250	60	10	1	-0.03	0.12	-10.00	3.89
250	60	15	1	0.02	0.18	3.61	49.60
250	60	20	1	0.05	0.24	4.38	37.38
250	60	25	1	0.01	0.30	16.67	16.67
250	90	1	1	0.01	0.01	0.59	26.12
250	90	5	1	-0.00	0.06	-9.20	6.39
250	90	10	1	-0.01	0.12	0.10	39.18
250	90	15	1	0.00	0.18	10.34	25.29
250	90	20	1	0.01	0.24	-15.63	-5.70
250	90	25	1	-0.03	0.30	-4.10	2.09

Table 5. Average lumbosacral spinal cord responses to focused ultrasound stimulation. Displays the following parameters for each set of conditions: (i) average change in MAP (mmHg) per each second that FUS is on, (ii) I_{spta} value, (iii) average change in MAP for total stimulation period, and (iv) the maximum increase in MAP from FUS stimulation. FUS stimulation period can span 15 to 90 s.

After a single period of FUS stimulation, the MAP returned to baseline in a few seconds. However, after several stimulation periods (segments), noticeable shifts in the MAP baselines were observed. This observation was characterized as a form of sensitization by the nervous system to the FUS stimulation. Following segments of lower-thoracic-level stimulation, MAP was shown to have an extended reduction relative to the baseline. Across the 7 parameter groups evaluated, there was a consistent decrease in MAP after FUS stimulation. In subsequent quantifications of the effects of FUS stimulation, the average timing for the MAP to return to baseline levels ranged from 112 to 600 s. Supplemental Table 6 outlines the mean return time to threshold for the varying amplitude and duty cycle parameters used in the thoracic spinal cord. Following segments of lumbosacral-level stimulation, MAP was shown to have a decreased baseline in rats that received FUS. Overall, an increasing delay to return was observed in lumbosacral stimulation segments. Lower duty cycle, approximately 1%, showed shorter periods of return to baseline, while higher duty cycles had return to baseline periods on the order of 120 to 600 s, similar to the thoracic stimulation. It should be noted that for all the animals used, over the hours of each experiment, the MAP baseline would decrease.

Autonomic tone is the interaction and balance of the sympathetic and parasympathetic nervous systems^{50,51}. Baseline autonomic tone could influence the responsiveness to stimulation. To assess autonomic tone and its contribution to the observed BP modulations, the peak-to-peak interval dynamics were compared before and after FUS stimulation with Poincaré plots^{52–54}. Scatter plots of successive peak-to-peak intervals demonstrated tighter clustering prior to stimulation, indicating a more regular rhythm, and greater dispersion after FUS, consistent with increased variability. Ellipse metrics from Poincaré analysis revealed moderate short-term variability (SD1) with more pronounced long-term fluctuations (SD2) (Fig. 7A). The overall low SD1/SD2 ratio indicates that variability was dominated by slower oscillations. These Poincaré results show that FUS induced measurable changes in HRV, characterized by expanded peak-to-peak interval dispersion and enhanced long-term variability. The increase along the SD2 axis suggests altered autonomic modulation, potentially reflecting baroreflex involvement or increased parasympathetic input, while short-term variability remained relatively stable. Figure 7B shows the average SD1/SD2 ratio for the rats in their respective stimulation sites. Statistical significance was observed across spinal region using one sample t-tests in both thoracic ($P < 0.001$) and lumbosacral ($P = 0.0485$) groups.

An exponential fit was applied to the data to quantify the post-stimulation FUS effect on the MAP (Supplemental Fig. 4). This was done because the MAP response to FUS stimulation is not instantaneous and cannot be represented as a square function. For lower thoracic stimulation, where MAP decreased, the average exponential fit for the post-stimulation was as follows (where t is time):

$$MAP = -34.78e^{(-2.33t)} \quad (1)$$

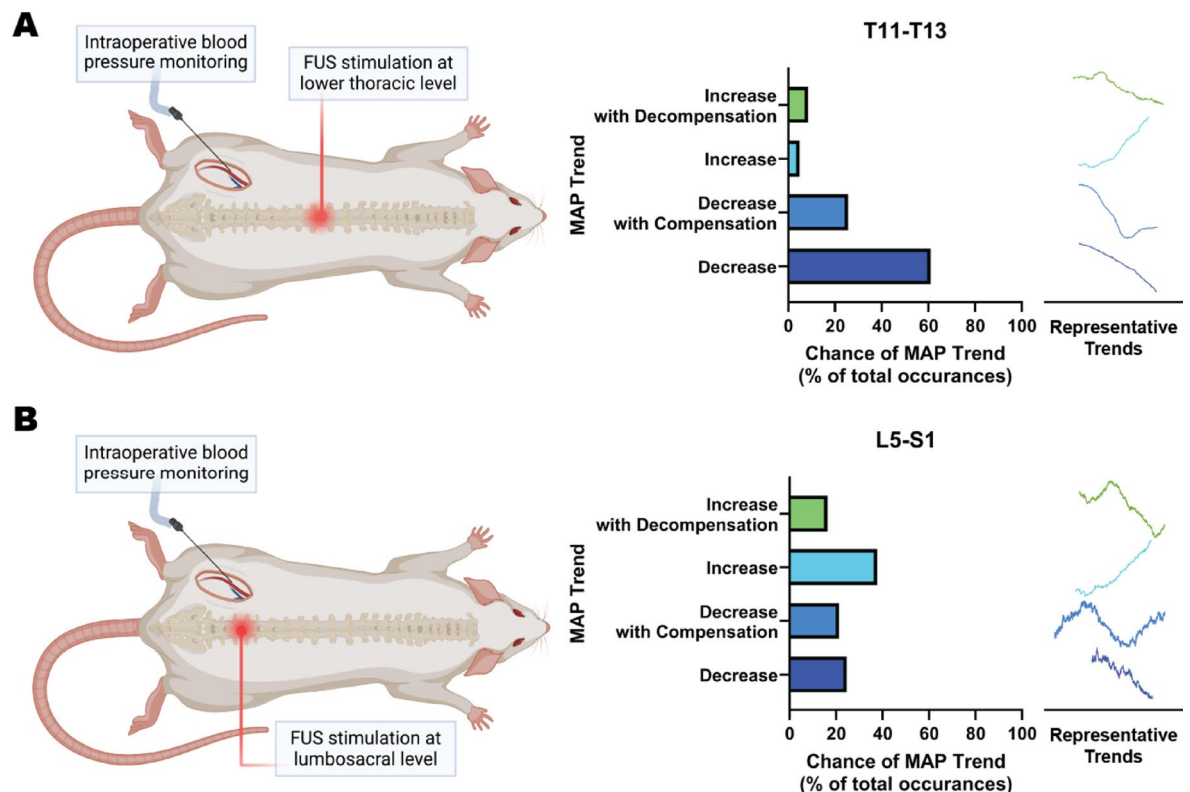


Fig. 4. Probability of event in rat BP changes from FUS stimulation on naïve spinal cord. **(A)** Schematic overview of intraoperative modulation at the lower thoracic level. The event probabilities at lower thoracic levels (T11-T13; 4 rats, n = 82 instances of stimulation) are shown on the right. **(B)** Schematic overview of intraoperative modulation at the lumbosacral level. The event probabilities at lumbosacral levels (L5-S1; 4 rats, n = 61 instances of stimulation) are shown on the right. Created in BioRender. Thakor, 2025) <https://BioRender.com/itb5fd5>.

For lumbosacral stimulation, where MAP increased, the average exponential fit for the post-stimulation was as follows (where t is time):

$$MAP = -8.23e^{(0.15t)} \quad (2)$$

Ultimately, these average post-stimulation fittings help distinguish how the FUS stimulation response is represented in the MAP. These equations could be further applied in future models for automated stimulation, to react to patient MAP and correspondingly turn on FUS stimulation.

Porcine model with FUS

To assess the translational potential of our findings beyond the rodent model, we evaluated the FUS stimulations on a Yorkshire pig. This pig yielded 31 instances of FUS stimulation. The large animal model provides enhanced anatomical similarity to human spinal cord dimensions and physiological responses, which can stage for a more comprehensive translation of FUS-mediated MAP modulation and physiological effects to large animal models and humans. Stimulation was done with repeated alternation between a FUS stimulation period and a washout period over several hours. Again, the washout periods were to allow sufficient time for the pig to return to baseline and for stimulation effects to dissipate. At the thoracic spinal cord sonication sites, the FUS stimulations yielded a Decrease in MAP for 10% (Fig. 8). There was a subsequent 6% of thoracic events that had Decrease With Compensation. Meaning, an overall 16% of FUS stimulation events yielded a type of decrease in MAP. Consistent with our rodent findings, thoracic spinal cord FUS stimulation in the porcine model produced comparable reductions in MAP (Supplemental Table 5). These results suggest cross-species reproducibility of the observed hemodynamic responses to FUS neuromodulation. While it is encouraging to see the results from rats translate to a larger animal model, further research in a porcine model might reveal more species-dependent differences. It should be noted that 65% of pig stimulations yielded no change in blood pressure, highlighting that parameters cannot be directly extrapolated across species and that pig-specific parameter optimization will be necessary. This could be important for future translational studies in humans.

The pig spinal cord sections were evaluated for overall structural integrity and general tissue analysis. Figure 9A is a representative histological image from spinal cord samples in the upper thoracic vertebral level. The upper thoracic level in the pig received lower intensity parameters of the FUS stimulation. Here, it is noted that the anterior horns remain intact and the central canal, peripheral nerve, and nerve roots are unremarkable.

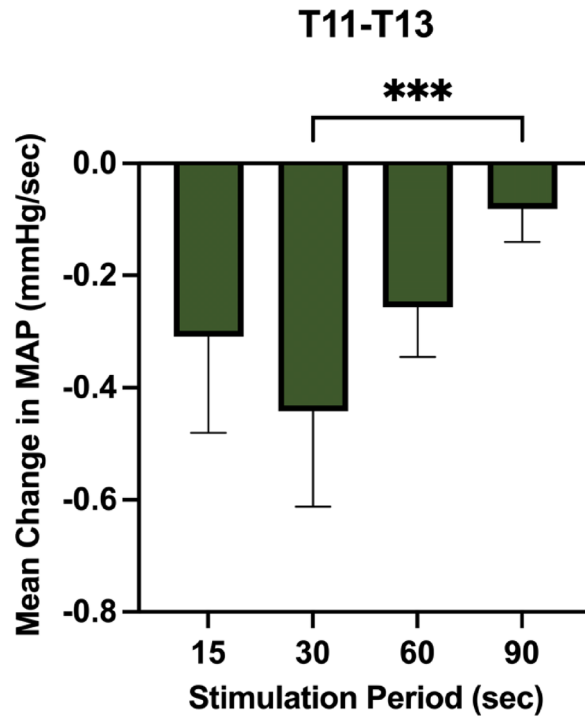


Fig. 5. Mean change in MAP after FUS stimulation at lower thoracic spinal cord level. The figure depicts the average change in MAP for one second of stimulation ($n = 4$ rats). Four stimulation periods were evaluated: 15, 30, 60, and 90 s. A one-way between-subjects ANOVA showed that a 30-s FUS stimulation period was more effective at inducing a neuromodulatory change in MAP compared with a 90-s FUS stimulation period; $\alpha = 0.05$; $***P = 0.0005$.

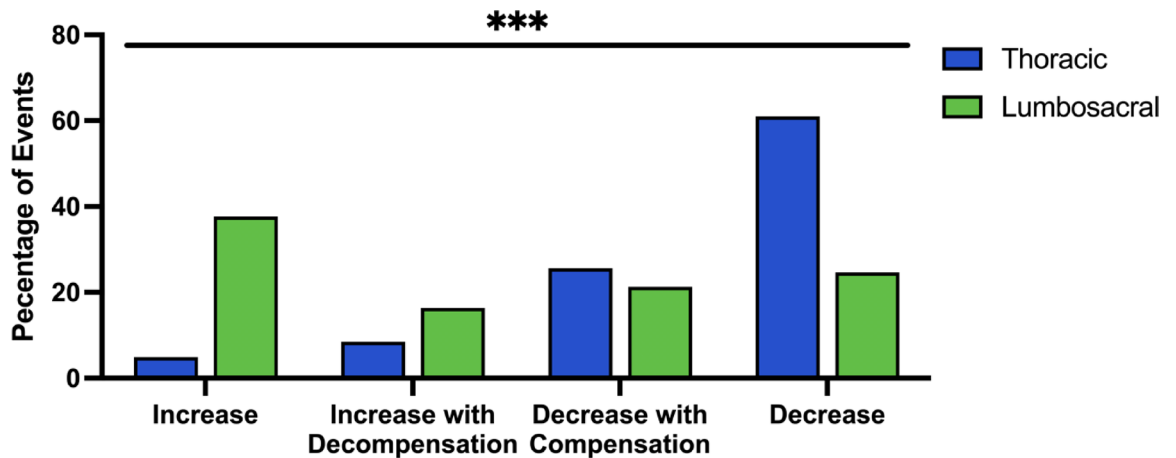


Fig. 6. Distribution of FUS-induced MAP event classification across spinal regions. We evaluated $n = 82$ instances of stimulation in the thoracic region (T11-T13, $n = 4$) and $n = 61$ instances in the lumbosacral region (L5-S1, $n = 4$). There was a statistically significant difference in frequencies between the spinal regions; $***$ Chi-squared and Fisher's exact $P < 0.001$.

There is mild dilation of the vasculature, which is seen in the blood vessels of the darker, gray matter horn. This dilation can provide insight into the possible cellular mechanism of FUS stimulation. As we mentioned, thoracic neuromodulation sees a decrease in MAP. Dilation of these vessels would aid in this decrease in MAP. Figure 9B is a representative histological image from spinal cord samples in the lower thoracic vertebral level. The lower thoracic level in the pig received higher intensity parameters of the FUS stimulation. The section shows some subarachnoid hemorrhage in the meninges, marked dilatation of parenchymal vessels, and degeneration of the central spinal cord tissue. Notable ablative changes were observed in this tissue. This demonstrates the baseline

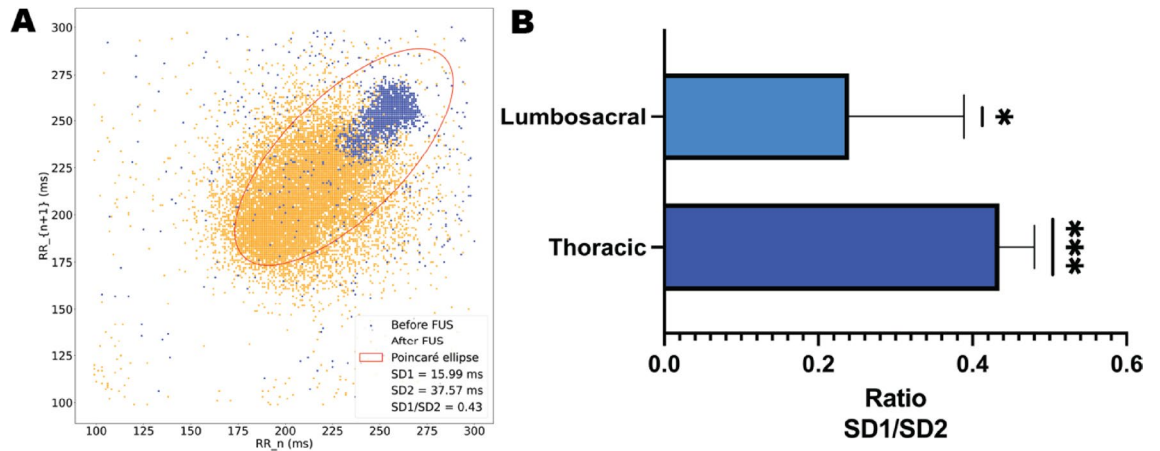


Fig. 7. Intraoperative cardiovascular monitoring. **(A)** The representative Poincaré plot depicts the difference in subject heart rate pre- and post-FUS stimulation. **(B)** The bar graph illustrates the ratio of SD1/SD2 for the 8 rats (4 thoracic, 4 lumbosacral) from their corresponding Poincaré plots; one sample t-test and Wilcoxon test *** $P=0.0003$, * $P=0.0485$.

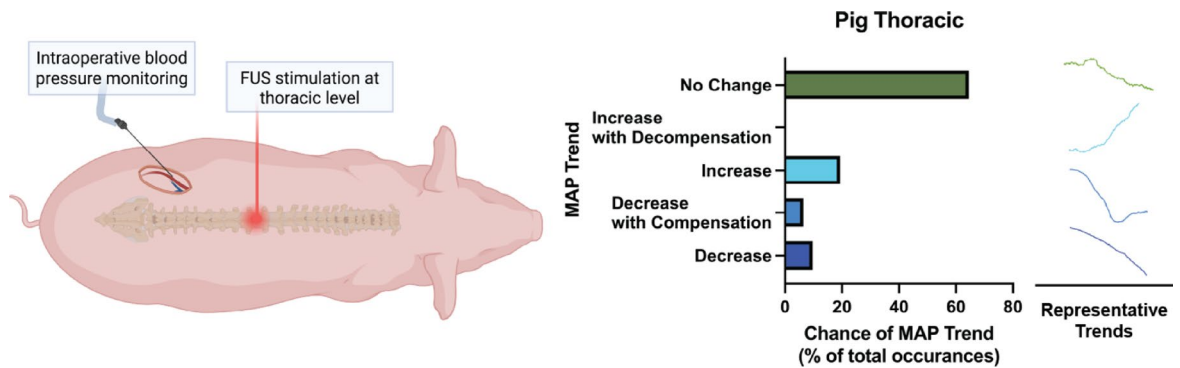


Fig. 8. Probability of event in pig BP changes from FUS stimulation on naïve spinal cord. Schematic overview of intraoperative modulation at the thoracic level. The event probabilities at lower and upper thoracic levels (1 pig, $n = 31$ instances of stimulation) are shown on the right. This includes LIFU and HIFU stimulation of the pig spinal cord. Created in BioRender. Thakor, (2025) <https://BioRender.com/itb5fd5>.

physiological effect of the FUS stimulation. Long term physiological impact and safety were not explored in this study.

Discussion

Physiological significance

This study establishes the observational results of FUS stimulation to the spinal cord. The coaxial ultrasound system is unique in its live visualization of the FUS beam profile and focal point (Supplemental Fig. 2). The novel observations of FUS stimulation leading to decreases or increases in MAP have led to more questions and hypotheses about the cellular mechanism of action^{55,56}. The contrast in physiological responses from the lower thoracic level and the lumbosacral level is thought to be driven by the distinct interplay of sympathetic and parasympathetic innervations. The lower thoracic level is characterized by significant sympathetic and parasympathetic innervation. The lumbosacral level, meanwhile, features predominantly parasympathetic innervation. We hypothesize that the FUS stimulation described here inhibits neuronal activity, enabling targeted MAP modulation through level-specific stimulation. This hypothesis aligns with our previous work, in which FUS was found to inhibit spinal cord pathways³⁶. There could also be confounding factors accounting for the decrease, which would not be attributed to FUS stimulations alone. Our findings align with previous work demonstrating segment-specific modulation of descending motor pathways via trans-spinal FUS⁵⁷. This suggests that FUS could be a versatile neuromodulatory technique for both autonomic and somatic circuits through precise anatomical targeting. Further research may provide a deeper understanding of the cellular mechanisms underlying FUS stimulation on the spinal cord.

In reference to the pig spinal cord histology, the general ablative effect of HIFU stimulation is overt. Future studies will discern additional safety indications associated with each FUS stimulation parameter. With the completed studies, we observed that with low enough intensity, the spinal cord tissue remains intact and shows

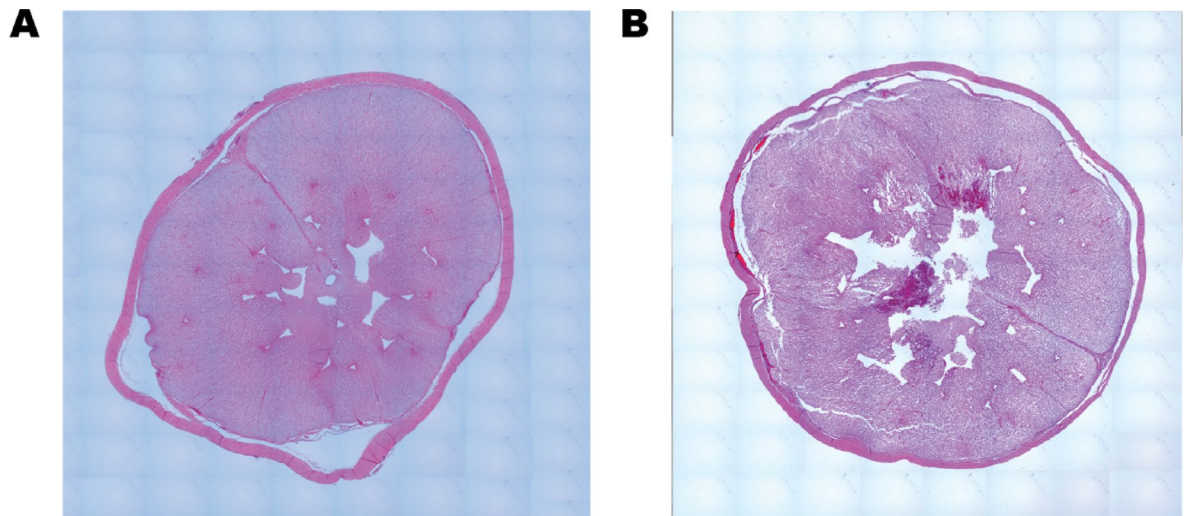


Fig. 9. Representative histological images of pig spinal cord after receiving a therapeutic FUS stimulation. **(A)** Thoracic spinal cord after receiving low-intensity FUS (n = 1 pig). **(B)** Thoracic spinal cord after receiving high-intensity FUS (n = 1 pig).

dilation of its vasculature. Here, we utilized ultrasound with a power that is greater than diagnostic imaging but less than ablative HIFU parameters. Stimulation parameters regarding power and specific intensity will need to be optimized before clinical translation.

The dichotomy in modulatory responses between the lower thoracic and lumbosacral regions opens intriguing insights into the mechanisms of the two pathways. Although others have studied various aspects of FUS neuromodulation, the cellular mechanism behind the modulation remains unknown. Some evidence suggests that the mechanistic pathway involves no thermal component at a low-intensity FUS stimulation^{14,15}. It has been shown that FUS can influence ion-channel regulation and activate mechanical receptors in the neurons^{25,58}. In this study, the fundamental focal width of the focused ultrasound is 3.02 mm and the rat spinal cord cross section ranges from 2.5–3.5 mm. The width of the focused ultrasound beam being similar in size to the cross section of a rat spinal cord suggests that FUS stimulation at one vertebral level could also affect projections to adjacent levels. This should be noted, as there could be a possibility of non-specific activation from FUS stimulation. The single pig is limited in its LIFU translatability from the rats as the predominant rat parameters elicited little to no change in the pig's blood pressure. This highlights the possible need for higher acoustic intensity in larger models. Ultimate implementation in a clinical setting would require its use to be minimally invasive or non-invasive. Though this study utilizes FUS in an invasive, surgical approach, the technology has the potential to emerge as a minimally invasive therapy for BP management.

LIFU could inhibit neuronal activity in a similar manner, reducing neuronal firing at the thoracic and lumbosacral levels^{59,60}. This inhibition of neuron firing explains the changes in MAP. The lumbosacral vertebrae are innervated mainly by parasympathetic neurons. As a result, inhibition at these levels would lead to relative sympathetic predominance, as reflected in the MAP increases observed and vasoconstriction. The lower thoracic vertebrae are innervated by a combination of sympathetic and parasympathetic neurons, and when inhibited, we see a decrease in MAP. This suggests one of two scenarios. Either A) FUS inhibits sympathetic neurons more than parasympathetic neurons, or B) the lower thoracic vertebrae in rats and pigs have a greater percentage of sympathetic innervation than parasympathetic. In the latter scenario, when both pathways are inhibited, the summative result is a decrease in MAP. There are still limitations to our understanding of the differences between local and systemic MAP. In cases of SCI, it is thought that recruitment of blood flow to the site of injury is best for patient recovery. Current methods of increasing blood flow involve increasing the MAP, thereby necessitating a comprehensive investigation of regional spinal cord MAP dynamics following injury.

It should be noted that the chronic effects of such a model were not explored within this study. Long-term safety studies are warranted to establish the lasting effects of FUS and to investigate the immune response that may be elicited before the technology can be translated to humans. Prior investigations in tumor treatments have demonstrated that immune responses can be elicited with FUS stimulation, particularly at high-intensity acoustic parameters and with the use of microbubbles^{61–63}. In the setting of spinal cord injury, FUS has the potential to modulate immune responses and promote recovery; however, the field is still in its infancy and requires additional investigation⁶⁴.

Clinical translation

Traumatic SCI dramatically decreases an individual's quality of life, causing loss of motor function, sexual function, and bowel control^{65,66}. Acute SCI management involves surgical decompression via laminectomy to alleviate spinal cord compression and subsequent inflammation^{12,13,66–69}. In some cases, SCI can lead to the development of autonomic dysreflexia (AD), a life-threatening syndrome consisting of episodes of uncontrolled hypertension triggered by a stimulus below the site of injury. Current AD management relies predominantly on

pharmacological agents, which are associated with significant adverse effects, including rebound hypotension, cephalgia, and vertigo, plus diminished therapeutic efficacy over time⁸. These limitations highlight the need for more reliable MAP management options. Our experimental findings demonstrate that FUS stimulation of the spinal cord effectively modulates MAP. Further evaluation will help maximize FUS neuromodulation as a safe and non-systemic intervention for frequent AD episodes and chronic BP disorders.

Conclusion

We have demonstrated that therapeutic FUS stimulation of the spinal cord causes changes in MAP. The studies outlined in this paper illustrate the development of FUS for BP modulation. To date, we have implemented FUS stimulation and assessed its implementation on an exposed spinal cord in both rodent and porcine models. The observations demonstrate that FUS can have region-specific modulation outcomes in the spinal cord. Future research may focus on optimizing transducer design, stimulation parameters, FUS probe localization, power delivery, and evaluating patient safety. Our findings establish the foundation for considering LIFU as a therapeutic modality for MAP regulation via spinal cord neuromodulation. LIFU's effects on spinal cord are observed to affect both increase in MAP and reduction as well depending on the target site. Thus, how the FUS probes are implemented and where they are placed will need optimization for appropriately targeted clinical applications.

Data availability

The data supporting the results of this study are available within the paper and its Supplementary Information. All data generated in this study will be made available. For data, please contact Angelica Lopez (alopez47@jh.edu) and Amir Manbachi (amir.manbachi@jh.edu).

Code availability

The code used in this manuscript for statistical analysis will be made available on GitHub at the following domain: <https://github.com/af008/bpfus>. Please contact Angelica Lopez (alopez47@jh.edu) for questions and access.

Received: 27 June 2025; Accepted: 20 October 2025

Published online: 21 November 2025

References

1. Pressure, H. B. High Blood Pressure Facts | cdc.gov. Centers for Disease Control and Prevention. 24–6. (2025) <https://www.cdc.gov/bloodpressure/facts.htm>
2. World Health Organization (WHO). Hypertension 16. World Health Organisation. 4–7. (2023) <https://www.who.int/news-room/fact-sheets/detail/hypertension>
3. Chobufo, M. D. et al. Prevalence and control rates of hypertension in the USA: 2017–2018. *Int. J. Cardiol. Hypertens.* **6**, 100044. <https://doi.org/10.1016/J.IJCHY.2020.100044> (2020).
4. Hypertension (2025). <https://www.who.int/news-room/fact-sheets/detail/hypertension>. Accessed 1 Jun 2025.
5. Managing High Blood Pressure | High Blood Pressure|CDC (2025). <https://www.cdc.gov/high-blood-pressure/living-with/index.html>. Accessed 1 Jun 2025.
6. How to Manage High Blood Pressure | American Heart Association (2025). <https://www.heart.org/en/health-topics/high-blood-pressure/changes-you-can-make-to-manage-high-blood-pressure>. Accessed 1 Jun 2025.
7. High Blood Pressure—Treatment | NHLBI, NIH. (2025) <https://www.nhlbi.nih.gov/health/high-blood-pressure/treatment>. Accessed 1 Jun 2025.
8. Krassioukov, A., Warburton, D. E., Teasell, R. & Eng, J. J. A systematic review of the management of autonomic dysreflexia after spinal cord injury. *Arch. Phys. Med. Rehabil.* **90**, 682–695. <https://doi.org/10.1016/j.apmr.2008.10.017> (2009).
9. Ahmad, H. et al. Angiotensin-converting enzyme and hypertension: A systemic analysis of various ACE inhibitors, their side effects, and bioactive peptides as a putative therapy for hypertension. *J. Renin Angiotensin Aldosterone Syst.* **023**, 7890188. <https://doi.org/10.1155/2023/7890188> (2023).
10. DeMers, D. & Wachs, D. Physiology, Mean Arterial Pressure. StatPearls. StatPearls Publishing, (2023). <https://www.ncbi.nlm.nih.gov/books/NBK538226/>. Accessed 2 Jun 2025.
11. Brzezinski, W. A. Blood Pressure. *Clinical Methods: The History, Physical, and Laboratory Examinations*. Butterworths. (1990). <https://www.ncbi.nlm.nih.gov/books/NBK268/>. Accessed 19 Jun 2025.
12. Walters, B. C. et al. Guidelines for the management of acute cervical spine and spinal cord injuries: 2013 update. *Neurosurgery* **60**, 82–91. <https://doi.org/10.1227/01.neu.0000430319.32247.7f> (2013).
13. Hadley, M. N. Blood pressure management after acute spinal cord injury GUIDELINES : There is insufficient evidence to support treatment guidelines. *Options Neurosurg.* **50**, 58–62 (2002).
14. O'Brien, W. D. Ultrasound-biophysics mechanisms. *Prog. Biophys. Mol. Biol.* **93**, 212–255. <https://doi.org/10.1016/j.pbiomolbio.2006.07.010> (2007).
15. ter Haar, G. Therapeutic applications of ultrasound. *Prog. Biophys. Mol. Biol.* **93**, 111–129. <https://doi.org/10.1016/j.pbiomolbio.2006.07.005> (2007).
16. Lynn JG, Zwemer RL, Chick AJ, Miller AE. A new method for the generation and use of focused ultrasound in experimental biology. (1942). <http://rupress.org/jgp/article-pdf/26/2/179/1239446/179.pdf>
17. Cheung, V. Y. T. High-intensity focused ultrasound therapy. *Best Pract. Res. Clin. Obstet. Gynaecol.* **46**, 74–83. <https://doi.org/10.1016/j.bpobgyn.2017.09.002> (2018).
18. Lei, T. et al. High-intensity focused ultrasound ablation in the treatment of recurrent ovary cancer and metastatic pelvic tumors: A feasibility study. *Int. J. Hyperth.* **38**, 282–287. <https://doi.org/10.1080/02656736.2021.1889698> (2021).
19. Phenix, C.P., Togtema, M., Pichardo, S., Zehbe, I., Curiel, L. High intensity focused ultrasound technology, its scope and applications in therapy and drug delivery. *J. Pharm. Pharm Sci.* (www.cspCanada.org). (2014).
20. Izadifar, Z., Izadifar, Z., Chapman, D. & Babyn, P. An introduction to high intensity focused ultrasound: Systematic review on principles, devices, and clinical applications. *J. Clin. Med. MDPI* <https://doi.org/10.3390/jcm9020460> (2020).
21. Yin, Y., Pan, F., He, M., Zhang, C. & Liu, Y. High intensity focused ultrasound combined with ultrasound-guided suction curettage treatment for cesarean scar pregnancy: A comparison of different HIFU sonication strategies. *Int. J. Hyperth.* **39**, 390–396. <https://doi.org/10.1080/02656736.2022.2044078> (2022).

22. Meng, Y., Hynynen, K. & Lipsman, N. Applications of focused ultrasound in the brain: From thermoablation to drug delivery. *Nat. Rev. Neurol.* **17**, 7–22. <https://doi.org/10.1038/s41582-020-00418-z> (2021).
23. Blackmore, J., Shrivastava, S., Sallet, J., Butler, C. R. & Cleveland, R. O. Ultrasound Neuromodulation: A Review of Results. *Mech. Saf. Ultrasound Med. Biol.* **45**, 1509–1536. <https://doi.org/10.1016/j.ultrasmedbio.2018.12.015> (2019).
24. Meng, Y. et al. Focused ultrasound neuromodulation. 1st ed.. *Int. Rev. Neurobiol.* **1595**, 221. <https://doi.org/10.1016/bs.irm.2021.06.004> (2021).
25. Baek, H., Pahk, K. J. & Kim, H. A review of low-intensity focused ultrasound for neuromodulation. *Biomed. Eng. Lett.* **7**, 135–142. <https://doi.org/10.1007/s13534-016-0007-y> (2017).
26. Liao, Y. H. et al. Effects of noninvasive low-intensity focus ultrasound neuromodulation on spinal cord neurocircuits in vivo. *Evid. Based Complement. Altern. Med.* **202**, 8534466. <https://doi.org/10.1155/2021/8534466> (2021).
27. Lee, S. A., Kamimura, H. A. S., Burgess, M. T. & Konofagou, E. E. Displacement imaging for focused ultrasound peripheral nerve neuromodulation. *IEEE Trans. Med. Imaging NLM Medline* **39**, 3391–3402. <https://doi.org/10.1109/TMI.2020.2992498> (2020).
28. Walker, M. R. et al. Peripheral nerve focused ultrasound lesioning-visualization and assessment using diffusion weighted imaging. *Front. Neurol.* **12**, 673060. <https://doi.org/10.3389/fneur.2021.673060> (2021).
29. Rodríguez-Meana, B. et al. Assessment of focused ultrasound stimulation to induce peripheral nerve activity and potential damage in vivo. *Front. Neurol.* **15**, 1346412. <https://doi.org/10.3389/fneur.2024.1346412> (2024).
30. Fishman, P. S. & Fischell, J. M. Focused ultrasound mediated opening of the blood-brain barrier for neurodegenerative diseases. *Front. Neurol. Front. Media S.A.* <https://doi.org/10.3389/fneur.2021.749047> (2021).
31. Gasca-Salas, C. et al. Blood-brain barrier opening with focused ultrasound in Parkinson's disease dementia. *Nat. Commun.* **12**, 1–7. <https://doi.org/10.1038/s41467-021-21022-9> (2021).
32. Rezaei, A. R. et al. Focused ultrasound-mediated blood-brain barrier opening in Alzheimer's disease: long-term safety, imaging, and cognitive outcomes. *J. Neurosurg.* **139**, 275–283. <https://doi.org/10.3171/2022.9.JNS221565> (2023).
33. Rezaei, A. R. et al. Ultrasound blood-brain barrier opening and Aducanumab in Alzheimer's disease. *N. Engl. J. Med.* **390**, 55–62. <https://doi.org/10.1056/nejmoa2308719> (2024).
34. Ji, N. et al. Blood pressure modulation with low-intensity focused ultrasound stimulation to the vagus nerve: A pilot animal study. *Front. Media S. A.* **14**, 586424. <https://doi.org/10.3389/fmins.2020.586424> (2020).
35. Bhimreddy, M. et al. Disruption of the blood-spinal cord barrier using low-intensity focused ultrasound in a rat model. *J. Vis. Exp. Mylove Corp.* <https://doi.org/10.3791/65113> (2023).
36. Tschay, Y., Zeng, Y., Weber-Levine, C., Awosika, T., Kerensky, M., Hersh, A.M., et al. Low-intensity pulsed ultrasound neuromodulation of a rodent's spinal cord suppresses motor evoked potentials. In: *IEEE Trans Biomed Eng. Institute of Electrical and Electronics Engineers (IEEE)*. 1–11. (2023) <https://doi.org/10.1109/tbme.2022.3233345>
37. Canon Medical Systems USA. Transducers For Ultrasound Systems. (2018). <https://us.medical.canon/products/ultrasound/transducers/aplio-i-series/>
38. Treeby, B. E., Jaros, J., Rendell, A. P. & Cox, B. T. Modeling nonlinear ultrasound propagation in heterogeneous media with power law absorption using a k-space pseudospectral method. *J. Acoust. Soc. Am.* **131**, 4324–4336. <https://doi.org/10.1121/1.4712021> (2012).
39. Toossi, A. et al. Comparative neuroanatomy of the lumbosacral spinal cord of the rat, cat, pig, monkey, and human. *Sci. Rep.* **11**, 1–15. <https://doi.org/10.1038/s41598-021-81371-9> (2021).
40. Kumar, A., Punnoose, J., Leadingham, K. M. K., Kerensky, M. J., Theodore, N., Thakor, N. V., et al. A patient-specific preplanning treatment algorithm for focused ultrasound therapy of spinal cord injury. In: *International IEEE/EMBS Conference on Neural Engineering, NER. IEEE Computer Society.* (2023). <https://doi.org/10.1109/NER52421.2023.10123718>
41. Acoustic Properties » ITIS Foundation. (2025) <https://itis.swiss/virtual-population/tissue-properties/database/acoustic-properties/>. Accessed 1 Jun 2025.
42. Basso, D.M., Beattie, M.S. & Bresnahan, J.C. A Sensitive and Reliable Locomotor Rating Scale for Open Field Testing in Rats. <https://home.liebertpub.com/neu>. Mary Ann Liebert, Inc., Publishers. **12**, 1–21. (2009) <https://doi.org/10.1089/NEU.1995.12.1>
43. Brown C. Urethral catheterization of the female rat. *Lab Anim (NY)*. Nature Publishing Group. **40**, 111–2 (2011) <https://doi.org/10.1038/labana0411-111>
44. Routkevitch, D. et al. Non-contrast ultrasound image analysis for spatial and temporal distribution of blood flow after spinal cord injury. *Sci. Rep.* **14**, 1–15. <https://doi.org/10.1038/s41598-024-51281-7> (2024).
45. Fukutoku, T. et al. Sex-Related differences in anxiety and functional recovery after spinal cord injury in mice. *J. Neurotrauma* **37**, 2235–2243. https://doi.org/10.1089/NEU.2019.6929/ASSET/IMAGES/NEU.2019.6929_FIGURE4.JPG (2020).
46. Murphy, K. R. et al. A practical guide to transcranial ultrasonic stimulation from the IFCN-endorsed ITRUSST consortium. *Clin. Neurophysiol.* **171**, 192–226. <https://doi.org/10.1016/j.clinph.2025.01.004> (2025).
47. Martin, E. et al. ITRUSST consensus on standardised reporting for transcranial ultrasound stimulation. *Brain Stimul.* **17**, 607–615. <https://doi.org/10.1016/j.brs.2024.04.013> (2024).
48. Şen, T., Tüfekçioğlu, O. & Koza, Y. Mechanical index. *Anadolu Kardiyol. Derg.* **15**, 334–336. <https://doi.org/10.5152/akd.2015.6061> (2015).
49. Pasquinelli, C., Hanson, L. G., Siebner, H. R., Lee, H. J. & Thielscher, A. Safety of transcranial focused ultrasound stimulation: A systematic review of the state of knowledge from both human and animal studies. *Brain Stimul.* **12**, 1367–1380. <https://doi.org/10.1016/j.brs.2019.07.024> (2019).
50. Gruionu, G. et al. Heart rate variability parameters indicate altered autonomic tone in subjects with COVID-19. *Sci. Rep.* **14**, 1–16. <https://doi.org/10.1038/s41598-024-80918-w> (2024).
51. Curtis, B. M. & O'Keefe, J. Autonomic tone as a cardiovascular risk factor: The dangers of chronic fight or flight. *Mayo Clin. Proc.* **77**, 45–54. <https://doi.org/10.4065/77.1.45> (2002).
52. Guzik, P. et al. Correlations between the poincaré plot and conventional heart rate variability parameters assessed during paced breathing. *J. Physiol. Sci.* **57**, 63–71. <https://doi.org/10.2170/physiolsci.RP005506> (2007).
53. Buzas, A., Horvath, T. & Der, A. A novel approach in heart-rate-variability analysis based on modified poincaré plots. *IEEE Access* **10**, 36606–36615. <https://doi.org/10.1109/ACCESS.2022.3162234> (2022).
54. Tayel, M. & AlSaba, E. Poincaré plot for heart rate variability world academy of science, engineering and technology. *Int. J. Biomed. Biol. Eng.* **9**, 708–711 (2015).
55. Yoo, S., Mittelstein, D. R., Hurt, R. C., Lacroix, J. & Shapiro, M. G. Focused ultrasound excites cortical neurons via mechanosensitive calcium accumulation and ion channel amplification. *Nat. Commun.* **13**, 493. <https://doi.org/10.1038/S41467-022-28040-1> (2022).
56. Hoffman, B. U. et al. Focused ultrasound excites action potentials in mammalian peripheral neurons in part through the mechanically gated ion channel PIEZO2. *Proc. Natl. Acad. Sci. U. S. A.* **119**, e2115821119. https://doi.org/10.1073/PNAS.2115821119/SUPPL_FILE/PNAS.2115821119.SAPP.PDF (2022).
57. Kim, E., Kum, J. & Kim, H. Trans-spinal focused ultrasound stimulation selectively modulates descending motor pathway. *IEEE Trans. Neural Syst. Rehabilitation Eng.* **30**, 314–320. <https://doi.org/10.1109/TNSRE.2022.3148877> (2022).
58. Kubanek, J. et al. Ultrasound modulates ion channel currents. *Sci. Rep.* **6**, 24170. <https://doi.org/10.1038/srep24170> (2016).
59. Collins, M.N., Legon, W. & Mesce, K.A. The inhibitory thermal effects of focused ultrasound on an identified, single motoneuron. *eNeuro*. **8** (2021) <https://doi.org/10.1523/ENEURO.0514-20.2021>
60. Wainger, B. J. et al. Effect of ezogabine on cortical and spinal motor neuron excitability in amyotrophic lateral sclerosis: A randomized clinical trial. *JAMA Neurol.* **78**, 186–196. <https://doi.org/10.1001/jamaneurol.2020.4300> (2021).

61. Joiner, J. B. et al. Low-intensity focused ultrasound produces immune response in pancreatic cancer. *Ultrasound Med. Biol.* **48**, 2344–2353. <https://doi.org/10.1016/j.ultrasmedbio.2022.06.017> (2022).
62. Wu, F. High intensity focused ultrasound ablation and antitumor immune response. *J. Acoust. Soc. Am.* **134**, 1695–1701. <https://doi.org/10.1121/1.4812893> (2013).
63. van den Bijgaart, R. J. E. et al. Thermal and mechanical high-intensity focused ultrasound: perspectives on tumor ablation, immune effects and combination strategies. *Cancer Immunol. Immunother.* **66**, 247–258. <https://doi.org/10.1007/s00262-016-1891-9> (2017).
64. Hwang, B.Y., Mampre, D., Ahmed, A.K., Suk, I., Anderson, W.S., Manbachi, A., et al. Ultrasound in Traumatic Spinal Cord Injury: A Wide-Open Field. *Neurosurgery*. Oxford University Press. 372–82. (2021) <https://doi.org/10.1093/neuros/nyab177>
65. Perez, N. E., Godbole, N. P., Amin, K., Syan, R. & Gater, D. R. Jr. Neurogenic bladder physiology, pathogenesis, and management after spinal cord injury. *J. Pers. Med. Multidiscip.* **12**(6), 968. <https://doi.org/10.3390/JPM12060968> (2022).
66. Jia, X., Kowalski, R. G., Sciubba, D. M. & Geocadin, R. G. Critical care of traumatic spinal cord injury. *J. Intensiv. Care Med.* <https://doi.org/10.1177/0885066611403270> (2024).
67. Hersh, A. M. et al. Advancements in the treatment of traumatic spinal cord injury during military conflicts. *Neurosurg. Focus* **53**, 1–9. <https://doi.org/10.3171/2022.6.FOCUS22262> (2022).
68. Ahuja, C. S. et al. Traumatic spinal cord injury—Repair and regeneration. *Clin. Neurosurg.* **80**, S22–90. <https://doi.org/10.1093/neuros/nyw080> (2017).
69. Anjum, A. et al. Molecular sciences spinal cord injury: pathophysiology, multimolecular interactions, and underlying recovery mechanisms. *Int. J. Mol. Sci.* <https://doi.org/10.3390/ijms21207533> (2024).

Acknowledgements

A.F.L. and P.L.P. acknowledge support from the National Science Foundation Graduate Research Fellowship Program (NSF GRFP): award DGE-2139757. D.R. discloses funding from the National Institutes of Health, NIH T32 GM136577, and F30 HL168823. N.T. and A.M. disclose funding support from Defense Advanced Research Projects Agency, DARPA, Award Contract #N660012024075. A.M. acknowledges funding from the Johns Hopkins Institute for Clinical and Translational Research Clinical Research Scholars Program (KL2), administered by the National Center for Advancing Translational Sciences (NCATS), (NIH KL2 TR003099). N.V.T. acknowledges funding from NIH R01 HL139158 and R01 HL071568.

Author contributions

****Conceptualization:**** A.F.L., D.R., N.T., N.V.T., A.M. ****Methodology:**** A.F.L., D.R., P.J.K., R.J., A.T., Z.S., E.C.B., A.D.D. ****Validation and formal analysis:**** A.F.L., D.R., P.J.K., N.A.B., A.T., V.N.V. S.K., P.L.P., R.S.B., C.G.E. ****Investigation:**** A.F.L., D.R., R.J., P.J.K., Z.S., E.B., A.D.D., V.N.V., S.K. ****Resources:**** A.M., N.T., N.V.T. ****Data curation:**** A.F.L., D.R., R.J., P.J.K. ****Writing—Original draft:**** A.F.L., D.R., N.A.B., B.M.T., N.V.T., A.M. ****Writing—Review and Editing:**** all authors. ****Visualization:**** A.F.L. ****Supervision, project administration, and funding acquisition:**** B.M.T., N.T., N.V.T., A.M.

Declarations

Competing interests

The authors declare no competing interests.

Ethics approval

All animal experiments were conducted in compliance with the National Institutes of Health guide for the care and use of laboratory animals (NIH Publications No. 8023, revised 1978). The experimental protocols were approved by the Johns Hopkins University Animal Care and Use Committee. All methods were performed following the ARRIVE guidelines (Animal Research: Reporting of In Vivo Experiments).

Additional information

Supplementary Information The online version contains supplementary material available at <https://doi.org/10.1038/s41598-025-25330-8>.

Correspondence and requests for materials should be addressed to A.M.

Reprints and permissions information is available at www.nature.com/reprints.

Publisher's note Springer Nature remains neutral with regard to jurisdictional claims in published maps and institutional affiliations.

Open Access This article is licensed under a Creative Commons Attribution-NonCommercial-NoDerivatives 4.0 International License, which permits any non-commercial use, sharing, distribution and reproduction in any medium or format, as long as you give appropriate credit to the original author(s) and the source, provide a link to the Creative Commons licence, and indicate if you modified the licensed material. You do not have permission under this licence to share adapted material derived from this article or parts of it. The images or other third party material in this article are included in the article's Creative Commons licence, unless indicated otherwise in a credit line to the material. If material is not included in the article's Creative Commons licence and your intended use is not permitted by statutory regulation or exceeds the permitted use, you will need to obtain permission directly from the copyright holder. To view a copy of this licence, visit <http://creativecommons.org/licenses/by-nc-nd/4.0/>.

© The Author(s) 2025